Fermi National Accelerator Laboratory

FERMILAB-PUB-91/342-T

MAD/PH/684

December 1991

Full Tree-level Calculation of the $qq \to qqWZ$ Electroweak Process at Hadron Supercolliders

V. Barger,[1] Kingman Cheung,[1] T. Han,[2] A. Stange,[1]

D. Zeppenfeld[1]

[1] *Department of Physics, University of Wisconsin, Madison, WI 53706*

[2] *Fermi National Accelerator Laboratory, P. O. Box 500, Batavia, IL 60510*

ABSTRACT

We present a full Standard Model calculation of the $qq \to qqWZ$ electroweak process in pp collisions at the SSC, including W and Z leptonic decay correlations. We also analyze the backgrounds to this signal from $Zt\bar{t} \to ZW +$ jets and $q\bar{q} \to WZ+$ jets. Single forward jet-tagging and vetoing of events with ≥ 2 central jets can suppress the backgrounds with little effect on the signal. With $10\,\mathrm{fb}^{-1}$ integrated luminosity we expect 50 signal events and 30 background events.

Operated by Universities Research Association Inc. under contract with the United States Department of Energy

I. INTRODUCTION

The interest in WZ production at future hadron supercolliders is in testing the electroweak gauge sector. One aspect is the measurement of 3-boson couplings in inclusive WZ production which has been addressed previously[1]; such measurements mainly probe the gauge interactions in the transverse boson sector. Another major issue is the measurement of weak boson scattering amplitudes. Regardless of whether there exists a Higgs boson of light mass (< 600 GeV), gauge boson scattering in the TeV region will provide crucial information on the full nature of electroweak symmetry breaking and the four gauge boson couplings.

The scattering of longitudinal weak bosons is closely related to electroweak symmetry breaking[2]. The channel $Z_L Z_L$ probes Higgs-like dynamics, $W_L^{\pm} Z_L$ probes QCD-like dynamics (*e.g* a technirho resonance), and $W_L^{\pm} W_L^{\pm}$ tests the possibility of new strong interactions in the weak boson sector. Detection of a heavy Higgs signal in pp collisions has been a subject of long standing interest[3]. Recently comprehensive studies have been made of Higgs signals in weak boson scattering in both the ZZ[4, 5] and W^+W^-[6] channels with the conclusion that a Higgs boson can be detected if its mass is less than about 1 TeV.

Other theoretical studies considered the possibility of isolating the vector boson scattering subprocesses $W^+W^+ \to W^+W^+$ [7–10]. Although there are major backgrounds such as W bremsstrahlung in quark scattering[8, 11], $Wt\bar{t}$ [8] and $t\bar{t}$ production[8, 9], it was found that these backgrounds can be effectively suppressed by judicious event selection criteria involving the vetoing of hard central jets combined with lepton isolation cuts or jet-tagging. The resulting signal event rates are at interesting levels for high luminosity machines.

In this paper we focus our attention on a full calculation of the electroweak $qq \to qqWZ$ scattering channel in order to assess Standard Model (SM) expectations and thus permit the identification of new physics contributions in this channel should they exist. Here a substantial enhancement may occur over the SM rate if there exists a WZ resonance state such as a technirho of technicolor models[12]; such a resonance occurs mainly in the scattering of longitudinal vector

bosons[13–15]. In the absence of a resonant structure, one would like to test the predictions of the SM in this channel.

The pp inclusive cross section at the SSC for the $qq \to qqWZ$ signal with leptonic W and Z decays (imposing minimal jet momentum transfer and separation cuts of $Q^2 > 5$ GeV^2 and $\Delta R_{jj} > 0.7$ and minimal lepton acceptance cuts of $|y_\ell| < 2$, $p_T(\ell) > 25$ GeV) is 16 fb, much smaller than the $q\bar{q} \to WZ$ annihilation background of 140 fb in lowest order[16] (about 230 fb at $\mathcal{O}(\alpha_s)$[17]) and the $gg, q\bar{q} \to Zt\bar{t}$ background of 83 fb for $m_t = 140$ GeV. Even if we restrict the kinematic range to high WZ invariant masses, the dominance of the background remains. However, single forward jet-tagging provides a means to suppress the backgrounds with only a modest reduction of the signal. In order to correctly implement a forward jet-tag we must calculate next to leading order contributions to the backgrounds discussed above. We shall also impose a central jet veto to further suppress the $Zt\bar{t}$ background. Hereafter we denote the electroweak $qq \to qqWZ$ signal by EW and refer to $q\bar{q} \to WZ$ production with additional jets as the QCD background.

The EW signal in the SM is dominated by transversely polarized weak bosons. We can further veto the transverse WZ events but the remaining longitudinal WZ signal in the SM is exceedingly small; any observation of excess events with these selection criteria would necessarily indicate the presence of new physics.

The organization of the paper is as follows. In Section II we outline the full calculation of the $qq \to qqWZ$ electroweak signal. Special attention is given to the treatment of diagrams involving photons at low Q^2. We also discuss the calculation of the various backgrounds. Section III gives our results, describing the acceptance criteria needed to isolate the signal. Complete amplitude formulas for the signal processes are given in Appendix A. Appendix B details the calculation of the amplitudes for the subprocesses leading to $Zt\bar{t}$ jet production.

II. CALCULATION OF PROCESSES PRODUCING $W^{\pm}Z$ + JETS

Our primary focus is the study of $WZ \to WZ$ scattering which enters in the $qq \to qqWZ$ subprocesses; representative Feynman graphs are shown in Fig. 1. There are several sources of backgrounds that we need to consider. The annihilation process $q\bar{q} \to WZ$ is of some concern. However, the requirement of at least one forward jet in the final state (single forward jet-tagging) is very effective in suppressing this exclusive channel; QCD corrections which lead to WZj production with one very energetic forward jet are rather small, as we will demonstrate. A more worrisome background is $Zt\bar{t}$ production with subsequent decay of the top quark to a real W boson and a b quark. In order to assess the efficiency of single jet-tagging it is necessary to include gluon emission contributions to this subprocess: the gluon jet has a larger probability to occur in the forward region than any of the top decay products.

In the following we elaborate on the techniques that we use in calculating these signal and background processes.

A. The $qq \to qqWZ$ signal

At $\mathcal{O}(\alpha^4)$, electroweak processes contribute significantly to $W^{\pm}Z$ production in association with two quarks that give up to two visible jets. A representative set of Feynman graphs for these processes is shown in Fig. 1. Our major interest is in the $WZ \to WZ$ scattering subprocesses such as the ones shown in Fig. 1(a) that include the $WWZZ$ four boson vertices. The Higgs boson enters only as a t-channel exchange contribution and the cross section is fairly insensitive to the value of the Higgs boson mass. As a reference value we choose $m_H = 0.1$ TeV, but also demonstrate the effect of changing this mass to 1 TeV. If a technirho resonance exists there would be additional $WZ \to WZ$ scattering graphs involving its exchange.

A complete tree-level calculation of $qqW^{\pm}Z$ production includes the contributions in which the weak bosons are radiated from external quark lines (see Figs. 1(b) and 1(c)). We have performed a full calculation using the helicity amplitude techniques of Ref. [18, 19]. Also included

in our calculation are the leptonic decays of the final state W- and Z-bosons. The full amplitude formulas are given in Appendix A.

Many aspects of the electroweak calculation for $qq \to qqWZ$ production are similar to those for $qq \to qqZZ$, qqW^+W^- and we refer the reader to our recent discussions of the latter[5, 6]. Particular care is required in treating low Q^2 photons such as occurs in the Feynman graph of Fig. 1(b). For $Q^2 < 5\,\mathrm{GeV}^2$ the parton calculation is inappropriate; instead the scattering of the virtual photon off the proton must be represented by the elastic and quasielastic structure functions of the proton. In a full calculation the available phase space for each of the final state quarks is separated into three regions, which are defined by the momentum transfer Q^2 and by the invariant mass W_{had} of the hadronic state which comprises the quark and the fragments of the proton from which this quark originates. In the deep inelastic region, defined by $Q^2 > 5\,\mathrm{GeV}^2$, the parton model is used. In the elastic region, defined by $W_{had} = m_p$, and the quasielastic region $Q^2 < 5\,\mathrm{GeV}^2$, $W_{had} > m_p + m_\pi$, which covers the rest, only photon exchange contributions are considered and the coupling of the photon to the proton is described by the dipole fit to the electric and magnetic elastic form-factors or by a parameterization of the experimentally determined low Q^2 quasielastic form-factor of the proton[20]. A comprehensive discussion of the procedure can be found in Ref. [21].

To estimate the size of the cross section below $Q^2 = 5\,\mathrm{GeV}^2$ we calculate the elastic processes $qp \to q'pWZ$, where p denotes the proton. Requiring the final state parton to have transverse momentum $p_T(j) > 40\,\mathrm{GeV}$, pseudorapidity $3 < |\eta_j| < 5$ and $E_j > 2$ TeV, this elastic WZ production cross section amounts to 0.23 fb as compared to 4.8 fb for the deep inelastic region. Thus the elastic contribution can be safely neglected. Similar studies of single W and Z production at ep colliders have shown that for a Q^2 cut as low as $5\,\mathrm{GeV}^2$ the quasielastic contributions are generally substantially smaller than the elastic ones[21]. In view of this we can restrict our calculations to the deep inelastic regime, imposing a $Q^2 > 5\,\mathrm{GeV}^2$ cutoff.

As seen by each of the two incoming protons, the vector boson fusion graphs of Fig. 1(a) re-

semble deep inelastic lepton-proton scattering via charged current and neutral current exchange. This suggests scale choices in the structure functions which are given by the squares of the momentum transfers between each of the incoming and final state quarks. To a good approximation we can choose $Q^2 = M_W^2$, as is common practice[10]. For the parton distribution functions we use the parameterization HMRS(B) of Harriman *et al.*[22].

In determining the acceptance of the $qq \to qqWZ$ signal we consider the second final state parton (after forward jet-tagging) as a candidate for a central jet, but we do not take into account additional central parton radiation from higher order QCD processes. In the lowest order $qq \to qqWZ$ process the two final state quarks have an average transverse momentum $p_T \approx \mathcal{O}(M_W)$. Any additional radiation of partons with $p_T \gtrsim M_W/2$ occurs via hard processes which will be suppressed by additional powers of α_s and hence should be only a small fraction of the inclusive cross section.

The $WZ \to WZ$ scattering rate has been estimated in Refs. [13,14] using the Effective W-boson Approximation (EWA). Because the distributions of transversely polarized vector bosons depend logarithmically on an undetermined scale, results based on the EWA have large uncertainties. Comparing with our exact calculations, the previous results significantly overestimate the $W_T Z_T$ scattering cross section.

B. The QCD WZj background

The forward jet required for tagging the signal can also arise by QCD radiation in the annihilation process $q\bar{q} \to WZ$ or from crossing related subprocesses. For the single jet-tagging that we shall use, a full tree-level calculation is required of the channnels

$$q\bar{q} \to WZg\,, \tag{1a}$$

$$qg \to WZq\,, \tag{1b}$$

$$\bar{q}g \to WZ\bar{q}\,. \tag{1c}$$

The relevant formulas have been presented previously in Refs. [23, 24].

Gluon emission from a quark leg leads to both infrared and collinear singularities in the tree level cross section formulas. These singularities can be avoided by implementing experimental acceptances in the calculation. We impose a cut on the jet transverse momentum of $p_T(j)_{min} = 40$ GeV and require the jet to have a pseudorapidity $|\eta_j| < |\eta_j|_{max} = 5$ in order to regularize the soft and collinear divergencies. We choose a scale $Q^2 = M_{WZ}^2$ in both the strong coupling constant α_s and in the structure functions for all our QCD WZj background calculations.

C. The $Zt\bar{t}g$ and $Zt\bar{t}q$ backgrounds

Additional sources for final states with a W and a Z boson are the subprocesses

$$gg, q\bar{q} \to Zt\bar{t}\,, \tag{2}$$

with $t \to bW$ decays. A possible distinguishing characteristic is the presence of additional final state jets from the b quarks in the top decay or from the hadronic decay of the second W. Formulas for the amplitudes of these subprocesses are given in Ref. [25].

This lowest order $Zt\bar{t}$ process often fails to provide a fast forward jet-tagging candidate. For that purpose we need to also consider the radiation of an additional gluon (or associated crossed diagrams):

$$gg, q\bar{q} \to Zt\bar{t}g\,, \tag{3a}$$

$$qg \to Zt\bar{t}q\,, \tag{3b}$$

$$\bar{q}g \to Zt\bar{t}\bar{q}\,. \tag{3c}$$

The corresponding helicity amplitudes are given in Appendix B.

We wish to calculate the $Zt\bar{t}$ background in such a way that it generates the dynamical distributions of the $\mathcal{O}(\alpha_s^3)$ processes and also reproduces the lowest order $Zt\bar{t}$ cross section when the extra parton becomes soft. In the following we use 'g' as a generic label of the extra parton

in $Zt\bar{t}$ events. The "poor person's shower" (PPS) approximation[26] incorporates the above features. The tree-level $Zt\bar{t}+1$ 'gluon' differential cross section $d\sigma(Zt\bar{t}g')_{\rm TL}$ is replaced by

$$d\sigma(Zt\bar{t}g')_{\rm PPS} = d\sigma(Zt\bar{t}g')_{\rm TL}\left(1-e^{-cp_{T_g}^2}\right)\ , \tag{4}$$

with the constant c properly chosen to reproduce the lowest order $Zt\bar{t}$ total cross section in the phase space region defined by our lepton acceptance cuts

$$|y_\ell| < 2\ , \qquad p_T(\ell) > 25\,{\rm GeV}\ . \tag{5}$$

As $p_{T_g} \to 0$ the final factor in Eq. (4) acts as a regulator on the extra parton. For $m_t = 140\,{\rm GeV}$, we find that $c = \left(\frac{1}{35\,{\rm GeV}}\right)^2$ gives the desired result at the SSC energy. In effect our calculations are very insensitive to this regulator. If the final state 'g' has $p_T(\text{'}g\text{'}) > 40\,{\rm GeV}$, as we will require for a jet, then the regulator in Eq. (4) is nearly unity and otherwise it does not affect the kinematic distributions very much. In the parton distributions and in α_s we choose one quarter of the $Zt\bar{t}$ invariant mass squared as the Q^2 scale. For all our considerations we take $m_t = 140$ GeV.

The $t \to Wb$, $W \to f\bar{f}'$ decays are fully implemented at the amplitude level. Hence the distributions of the final state particles in $t \to Wb \to \ell\nu b$ decays include full spin correlations in the decay matrix elements and all the polarization effects of the parent top quarks.

III. SIGNAL AND BACKGROUND COMPARISONS

In our calculations we shall impose the lepton acceptance of Eq. 5 and require

$$|\eta_j| < 5\ , \qquad p_T(j) > 40\ {\rm GeV}\ , \qquad \Delta R_{jj} > 0.7 \tag{6}$$

for all partons to be identified as jets; here $\Delta R_{jj} = \sqrt{(\Delta\phi)^2+(\Delta\eta)^2}$ is the separation between jets in the azimuthal angle – pseudorapidity plane. In the actual SSC experiments the p_T requirement will eliminate jets caused by fluctuations in the minimum bias background.

The energy distribution of the highest energy forward jet with pseudorapidity $3 < |\eta_j| < 5$ is shown in Fig. 2 for the EW, QCD, and $Zt\bar{t}g'$ contributions. The integrated cross sections

over this phase space region are roughly the same for the three contributions and the signal to background ratio is only 1:2.4. The requirement that the forward jet be energetic is effective in suppressing the backgrounds. When $E_j(\text{tag}) > 2$ TeV is imposed the signal to background ratio improves to almost 1:1 (see Table I).

A further improvement comes from the consideration of jet activity in the central region. In $Zt\bar{t}$'g' events there are extra central jets due to the b quarks in $t \to bW$ decays and the dijet from the decay of the second W. On the other hand the EW signal and the QCD background will have little central jet activity; the dominant feature of the EW signal is the two final state jets arising from $qq \to qqWZ$ one of which is required to be forward. By rejecting events having two or more central jets with

$$|\eta_j| < 3\,, \qquad p_T(j) > 40 \text{ GeV}, \tag{7}$$

the $Zt\bar{t}$'g' background is substantially reduced as shown in Fig. 3. With $E_j(\text{tag}) > 2$ TeV and the central jet veto, the signal to background ratio is improved to 1.5:1. The cross sections after central jet-vetoing are also given in Table I.

The numbers presented in Table I are based on minimal cuts on the lepton transverse momenta. One might wonder whether the signal to background ratio could be improved by concentrating on high WZ invariant mass events. Due to the missing neutrino in leptonic W decays, the WZ invariant mass cannot be determined directly, and we can only use the cluster transverse mass, defined by[27]

$$M_T^2(\ell\ell\ell, \not{p}_T) = \left(\sqrt{M_{\ell\ell\ell}^2 + p_{T\ell\ell\ell}^2} + |\not{\mathbf{p}}_T|\right)^2 - (\mathbf{p}_{T\ell\ell\ell} + \not{\mathbf{p}}_T)^2\ . \tag{8}$$

After imposing a missing transverse momentum acceptance cut of $\not{p}_T > 75\,\text{GeV}$, we obtain the cluster transverse mass distributions in Fig. 4. Unfortunately the shapes of the signal and the QCD background do not differ substantially. Hence only a marginal improvement in signal to background ratio can be achieved by an M_T cut at the expense of reducing the signal rate, which already is very small due to the additional missing p_T cut.

A more promising possibility is the invariant mass distribution of the three final state charged leptons, which is illustrated in Fig. 5. Here the QCD background falls more rapidly with increasing $M(\ell\ell\ell)$ than the signal and a $M(\ell\ell\ell) > 300$ GeV cut improves the signal to background ratio to 2.2:1 (see Table I).

The preceding results were all based on $m_H = 100$ GeV for which the WZ scattering mainly involves transversely polarized weak bosons. For a heavy Higgs boson the production of longitudinal gauge bosons also occurs via the Higgs exchange diagram of Fig. 1(a). However, the increase in cross section is not great; with $m_H = 1$ TeV we find a signal cross section after forward jet-tagging and $n_j(\text{central}) \leq 1$ of 5.1 fb as compared to 4.8 fb with $m_H = 0.1$ TeV. When we veto all central jets of $p_T > 40$ GeV the corresponding cross sections are 1.8 fb and 1.6 fb, as summarized in Table II. The size of this enhancement due to the longitudinal contributions would not yield a statistically significant signal even if the backgrounds could be ignored. If there exist new contributions beyond the SM such as a technirho WZ resonance of technicolor models, we would expect a very significant enhancement in rate. Taking the model discussed in Ref. [14] for illustration, the rates can be estimated in the equivalent weak boson approximation. The cross section of resonant WZ production at SSC energy, with lepton acceptance cuts and the jet-tagging cut, is about 10 fb for $M_{\rho_T} = 1$ TeV, $\Gamma_{\rho_T} = 200$ GeV and about 3 fb for $M_{\rho_T} = 2$ TeV, $\Gamma_{\rho_T} = 500$ GeV. Any significant excess of events observed in the cluster transverse mass or $M(\ell\ell\ell)$ spectra above these SM calculations would indicate the presence of new physics.

ACKNOWLEDGMENTS

This research was supported in part by the University of Wisconsin Research Committee with funds granted by the Wisconsin Alumni Research Foundation, in part by the U. S. Department of Energy under Contract No. DE-AC02-76ER00881, and in part by the Texas National Research Laboratory Commission (TNRLC) under Grant No. RGFY9173. T. Han was supported by an SSC Fellowship from TNRLC under Award No. FCFY9116. Further support was also provided by the U. S. Department of Education under Award No. P200A10197.

APPENDIX A

This Appendix gives all the formulas used in the calculation of the SM electroweak subprocess $qq \to qqW^+Z$; $qq \to qqW^-Z$ can be obtained by CP conjugation. We give the helicity amplitude expressions for the scattering matrix elements in a general R_ξ gauge. For notations and conventions we refer the reader to Ref. [5, 6]. The Feynman graphs for the subprocess $qq \to qqW^+Z$ are shown in Fig. 6. In all diagrams $q_1 = u, c$ and $q'_1 = s, d$, and q_2 can be any flavor. In our calculation the fermion masses are neglected and in addition all CKM mixing angles are set to zero, which is a very good approximation for the process at hand. After summing over final state flavors a mixing angle dependence would only remain in subprocesses like $u\bar{d}$ and $u\bar{s}$ annihilation which do not contribute very strongly to the inclusive cross section.

In order to establish a brief notation for diagrams like those in Figs. 6(i) and 6(l) which involve a WWZ vertex attached to a fermion line, we introduce the ket and bra

$$|k_1 + k_2, p_1\rangle = \Gamma_\mu\Big(k_1, k_2;\, \epsilon(k_1), \epsilon(k_2)\Big) P_W^{\mu\nu}(k_1 + k_2) \times \frac{(\not{p}_1 - \not{k}_1 - \not{k}_2)_{-\sigma_1}}{(p_1 - k_1 - k_2)^2} (\sigma_\nu)_{\sigma_1} \chi_{\sigma_1}(\bar{p}_1) \tag{A1}$$

$$\langle p_2, k_1 + k_2| = \Gamma_\mu\Big(k_1, k_2;\, \epsilon(k_1), \epsilon(k_2)\Big) P_W^{\mu\nu}(k_1 + k_2) \times \chi^\dagger_{\sigma_1}(\bar{p}_2)(\sigma_\nu)_{\sigma_1} \frac{(\not{p}_2 + \not{k}_1 + \not{k}_2)_{-\sigma_1}}{(p_2 + k_1 + k_2)^2} \tag{A2}$$

where

$$P_W^{\mu\nu}(k) = g^{\mu\nu} + \frac{(1 - \xi) k^\mu k^\nu}{\xi k^2 - M_W^2}\,, \tag{A3}$$

gives the numerator of the W boson propagator in a general R_ξ gauge and

$$T^{\mu\nu\lambda}(k_1, k_2) = (k_1 - k_2)^\mu g^{\nu\lambda} + (2k_2 + k_1)^\nu g^{\mu\lambda} - (2k_1 + k_2)^\lambda g^{\mu\nu} \tag{A4}$$

$$\Gamma^\mu(k_1, k_2;\, X, Y) = T^{\mu\nu\lambda}(k_1, k_2) X_\nu Y_\lambda \tag{A5}$$

describe the three vector boson vertex.

The coupling strength of the vector bosons to the fermions are described by factor $g_\sigma^V(f)$. For the Z boson they are defined by

$$g_{\sigma_i}^Z(f) = \begin{cases} g_Z\,(T_{3f} - Q_f x_{\rm w}) & \text{for } \sigma_i = -1\ , \\ g_Z\,(-Q_f x_{\rm w}) & \text{for } \sigma_i = +1\ , \end{cases} \tag{A6}$$

where $g_Z = g/\cos\theta_{\rm w}$, $x_{\rm w} = \sin^2\theta_{\rm w}$, and the γ coupling is $g_\pm^\gamma(f) = e\,Q_f = g\,\sin\theta_{\rm w}\,Q_f$. The W-fermion coupling strength is nonzero only for chirality $\sigma_i = -1$ of the fermions,

$$g_-^W = \frac{g}{\sqrt{2}}\ . \tag{A7}$$

The individual amplitudes, corresponding to the Feynman graphs of Fig. 6 and the permutations of weak bosons indicated there, are then given by

$$\begin{aligned} i\mathcal{M}^{(a)} = \sum_{V=\gamma,Z} & g_{VWW} g_{ZWW} g_{\sigma_1}^W g_{\sigma_3}^V(q_2) F_0 D^W(p_1-p_2) D^V(p_3-p_4) D^W(k_1+k_2) \\ & \times \Gamma_\mu\left[k_1, k_2;\, \epsilon(k_1), \epsilon(k_2)\right] \\ & \times \Gamma_\nu\left[p_1-p_2, p_3-p_4;\, \left\langle p_2\left|(\sigma)_{\sigma_1}\right|p_1\right\rangle, \left\langle p_4\left|(\sigma)_{\sigma_3}\right|p_3\right\rangle\right] P_W^{\mu\nu}(k_1+k_2) \end{aligned} \tag{A8}$$

where

$$g_{VWW} = \begin{cases} e\cot\theta_{\rm w} & \text{for } V = Z \\ e & \text{for } V = \gamma \end{cases} \tag{A9}$$

$$\begin{aligned} i\mathcal{M}^{(b)} = \sum_{V=\gamma,Z} & g_{VWW} g_{ZWW} M_W^2 g_{\sigma_1}^W g_{\sigma_3}^V(q_2)\, F_0\, D^W(p_1-p_2)\, D^V(p_3-p_4) \\ & \times \frac{\xi}{\xi(k_1+k_2)^2 - M_W^2} \epsilon(k_1)\cdot\epsilon(k_2) \left\langle p_2\left|(\sigma_\mu)_{\sigma_1}\right|p_1\right\rangle \left\langle p_4\left|(\sigma^\mu)_{\sigma_3}\right|p_3\right\rangle \\ & \times \begin{cases} -\tan^4\theta_{\rm w} & \text{if } V = Z \\ \tan^2\theta_{\rm w} & \text{if } V = \gamma \end{cases} \end{aligned} \tag{A10}$$

$$i\mathcal{M}^{(c)} = \sum_{V=\gamma,Z} -g_{VWW} g_{ZWW} g^W_{\sigma_1} g^V_{\sigma_3}(q_2) F_0 D^W(p_1-p_2)\, D^V(p_3-p_4)$$
$$\times\Big[2\left\langle p_4\left|\left(\not\epsilon(k_2)\right)_{\sigma_3}\right|p_3\right\rangle\left\langle p_2\left|\left(\not\epsilon(k_1)\right)_{\sigma_1}\right|p_1\right\rangle - \left\langle p_2\left|\left(\not\epsilon(k_2)\right)_{\sigma_1}\right|p_1\right\rangle\left\langle p_4\left|\left(\not\epsilon(k_1)\right)_{\sigma_3}\right|p_3\right\rangle$$
$$-\epsilon(k_1)\cdot\epsilon(k_2)\left\langle p_2\left|(\sigma_\mu)_{\sigma_1}\right|p_1\right\rangle\left\langle p_4\left|(\sigma^\mu)_{\sigma_3}\right|p_3\right\rangle\Big] \tag{A11}$$

$$i\mathcal{M}^{(d)} = -\frac{g^2}{1-x_{\rm w}} M_W^2 g^W_{\sigma_1} g^Z_{\sigma_3}(q_2) F_0 D^H(p_1-p_2-k_1)\, D^W(p_1-p_2)\, D^Z(p_3-p_4)$$
$$\times\left\langle p_2\left|(\not\epsilon(k_1))_{\sigma_1}\right|p_1\right\rangle\left\langle p_4\left|(\not\epsilon(k_2))_{\sigma_3}\right|p_3\right\rangle \tag{A12}$$

$$i\mathcal{M}^{(e)} = \sum_{V=\gamma,Z} g_{VWW} g_{ZWW} g^W_{\sigma_1} g^V_{\sigma_3}(q_2) F_0 D^W(p_1-p_2)\, D^V(p_3-p_4)\, D^W(p_1-p_2-k_2)$$
$$\times\Gamma_\mu\left[p_1-p_2,-k_2;\left\langle p_2\left|(\sigma)_{\sigma_1}\right|p_1\right\rangle,\epsilon(k_2)\right]$$
$$\times\Gamma_\nu\left[p_3-p_4,-k_1;\left\langle p_4\left|(\sigma)_{\sigma_3}\right|p_3\right\rangle,\epsilon(k_1)\right]$$
$$\times P_W^{\mu\nu}(p_1-p_2-k_2) \tag{A13}$$

$$i\mathcal{M}^{(f)} = \sum_{V=\gamma,Z} g_{VWW} g_{ZWW} g^W_{\sigma_1} g^V_{\sigma_3}(q_2) M_W^2 F_0 D^W(p_1-p_2)\, D^V(p_3-p_4)$$
$$\times\frac{\xi}{\xi(p_1-p_2-k_2)^2-M_W^2}\left\langle p_2\left|\left(\not\epsilon(k_2)\right)_{\sigma_1}\right|p_1\right\rangle\left\langle p_4\left|\left(\not\epsilon(k_1)\right)_{\sigma_3}\right|p_3\right\rangle$$
$$\times\begin{cases}-\tan^4\theta_{\rm w} & \text{if } V=Z\\ \tan^2\theta_{\rm w} & \text{if } V=\gamma\end{cases} \tag{A14}$$

$$i\mathcal{M}^{(g)} = \sum_{V=\gamma,Z} F_0 g^W_{\sigma_1} g^V_{\sigma_3}(q_2)$$
$$\times\Big\{g^Z_{\sigma_3}(q_2)\, D^V(p_1-p_2-k_1)\, P_V^{\mu\nu}(p_1-p_2-k_1)$$
$$\times\left[\left\langle p_2\left|(\sigma_\mu)_{\sigma_1}\right|k_1p_1\right\rangle g^V_{\sigma_1}(q_1') + \left\langle p_2k_1\left|(\sigma_\mu)_{\sigma_1}\right|p_1\right\rangle g^V_{\sigma_1}(q_1)\right]$$
$$\times\left[\left\langle p_4\left|(\sigma_\nu)_{\sigma_3}\right|k_2p_3\right\rangle + \left\langle p_4k_2\left|(\sigma_\nu)_{\sigma_3}\right|p_3\right\rangle\right]$$
$$+D^V(p_3-p_4)\left\langle p_4\left|(\sigma_\mu)_{\sigma_3}\right|p_3\right\rangle$$

$$\times\Big[\Big\langle p_2k_2\Big|(\sigma^\mu)_{\sigma_1}\Big|k_1p_1\Big\rangle g^Z_{\sigma_1}(q_1')g^V_{\sigma_1}(q_1')+\Big\langle p_2\Big|(\sigma^\mu)_{\sigma_1}\Big|k_2k_1p_1\Big\rangle g^Z_{\sigma_1}(q_1')g^V_{\sigma_1}(q_1')$$
$$+\Big\langle p_2\Big|(\sigma^\mu)_{\sigma_1}\Big|k_1k_2p_1\Big\rangle g^Z_{\sigma_1}(q_1)g^V_{\sigma_1}(q_1')+\Big\langle p_2k_2k_1\Big|(\sigma^\mu)_{\sigma_1}\Big|p_1\Big\rangle g^Z_{\sigma_1}(q_1')g^V_{\sigma_1}(q_1)$$
$$+\Big\langle p_2k_1k_2\Big|(\sigma^\mu)_{\sigma_1}\Big|p_1\Big\rangle g^Z_{\sigma_1}(q_1)g^V_{\sigma_1}(q_1)+\Big\langle p_2k_1\Big|(\sigma^\mu)_{\sigma_1}\Big|k_2p_1\Big\rangle g^Z_{\sigma_1}(q_1)g^V_{\sigma_1}(q_1)\Big]\Big\} \tag{A15}$$

$$i\mathcal{M}^{(h)}=\sum_{V=\gamma,Z}-g_{VWW}F_0g^W_{\sigma_1}g^V_{\sigma_3}(q_2)$$
$$\times\Big\{g^Z_{\sigma_3}(q_2)D^W(p_1-p_2)D^V(p_1-p_2-k_1)P_V^{\mu\nu}(p_1-p_2-k_1)$$
$$\times\Gamma_\mu\left[-k_1,p_1-p_2;\ \epsilon(k_1),\Big\langle p_2\Big|(\sigma)_{\sigma_1}\Big|p_1\Big\rangle\right]\left[\Big\langle p_4\Big|(\sigma_\nu)_{\sigma_3}\Big|k_2p_3\Big\rangle+\Big\langle p_4k_2\Big|(\sigma_\nu)_{\sigma_3}\Big|p_3\Big\rangle\right]$$
$$+D^V(p_3-p_4)\,D^W(p_1-p_2-k_2)\,P_W^{\mu\nu}(p_1-p_2-k_2)$$
$$\times\Gamma_\mu\left[p_3-p_4,-k_1;\ \Big\langle p_4\Big|(\sigma)_{\sigma_3}\Big|p_3\Big\rangle,\epsilon(k_1)\right]$$
$$\times\left[\Big\langle p_2k_2\Big|(\sigma_\nu)_{\sigma_1}\Big|p_1\Big\rangle g^Z_{\sigma_1}(q_1')+\Big\langle p_2\Big|(\sigma_\nu)_{\sigma_1}\Big|k_2p_1\Big\rangle g^Z_{\sigma_1}(q_1)\right]\Big\} \tag{A16}$$

$$i\mathcal{M}^{(i)}=\sum_{V=\gamma,Z}-g_{ZWW}F_0g^W_{\sigma_1}g^V_{\sigma_3}(q_2)D^V(p_3-p_4)D^W(k_1+k_2)$$
$$\times\Big[g^V_{\sigma_1}(q_1)\Big\langle p_2,\ k_1+k_2\Big|(\sigma^\mu)_{\sigma_1}\Big|p_1\Big\rangle\Big\langle p_4\Big|(\sigma_\mu)_{\sigma_3}\Big|p_3\Big\rangle$$
$$+g^V_{\sigma_1}(q_1')\Big\langle p_2\Big|(\sigma^\mu)_{\sigma_1}\Big|k_1+k_2,\ p_1\Big\rangle\Big\langle p_4\Big|(\sigma_\mu)_{\sigma_3}\Big|p_3\Big\rangle\Big] \tag{A17}$$

$$i\mathcal{M}^{(j)}=-g^W_{\sigma_1}\left(g^W_{\sigma_3}\right)^2g_{ZWW}F_0D^W(p_1-p_2)\,D^W(p_1-p_2-k_2)\,P_W^{\mu\nu}(p_1-p_2-k_2)$$
$$\times\Gamma_\mu\Big[p_1-p_2,\ -k_2;\ \Big\langle p_2\Big|(\sigma)_{\sigma_1}\Big|p_1\Big\rangle,\ \epsilon(k_2)\Big]$$
$$\times\left[\Big\langle p_4k_1\Big|(\sigma_\nu)_{\sigma_3}\Big|p_3\Big\rangle\delta_{q_2,d}+\Big\langle p_4\Big|(\sigma_\nu)_{\sigma_3}\Big|k_1p_3\Big\rangle\delta_{q_2,u}\right] \tag{A18}$$

$$i\mathcal{M}^{(k)}=g^W_{\sigma_1}\left(g^W_{\sigma_3}\right)^2F_0\Big\{D^W(p_1-p_2)\Big\langle p_2\Big|(\sigma^\mu)_{\sigma_1}\Big|p_1\Big\rangle$$
$$\times\left[\Big(g^Z_{\sigma_3}(q_2)\Big\langle p_4k_1\Big|(\sigma_\mu)_{\sigma_3}\Big|k_2p_3\Big\rangle+g^Z_{\sigma_3}(q_2')\Big\langle p_4k_1k_2\Big|(\sigma_\mu)_{\sigma_3}\Big|p_3\Big\rangle\right.\right.$$

$$
\begin{aligned}
&+ g^Z_{\sigma_3}(q_2)\left\langle p_4 k_2 k_1 \left| (\sigma_\mu)_{\sigma_3} \right| p_3 \right\rangle \Big) \delta_{q_2,d} + \Big(g^Z_{\sigma_3}(q_2) \left\langle p_4 k_2 \left| (\sigma_\mu)_{\sigma_3} \right| k_1 p_3 \right\rangle \\
&+ g^Z_{\sigma_3}(q_2') \left\langle p_4 \left| (\sigma_\mu)_{\sigma_3} \right| k_2 k_1 p_3 \right\rangle + g^Z_{\sigma_3}(q_2) \left\langle p_4 \left| (\sigma_\mu)_{\sigma_3} \right| k_1 k_2 p_3 \right\rangle \Big) \delta_{q_2,u} \Big] \\
&+ D^W(p_1 - p_2 - k_2)\, P^{\mu\nu}_W(p_1 - p_2 - k_2) \\
&\times \left[\left\langle p_4 k_1 \left| (\sigma_\mu)_{\sigma_3} \right| p_3 \right\rangle \delta_{q_2,d} + \left\langle p_4 \left| (\sigma_\mu)_{\sigma_3} \right| k_1 p_3 \right\rangle \delta_{q_2,u} \right] \\
&\times \left[\left\langle p_2 \left| (\sigma_\nu)_{\sigma_1} \right| k_2 p_1 \right\rangle g^Z_{\sigma_1}(q_1) + \left\langle p_2 k_2 \left| (\sigma_\nu)_{\sigma_1} \right| p_1 \right\rangle g^Z_{\sigma_1}(q_1') \right] \Big\} \qquad \text{(A19)}
\end{aligned}
$$

$$
\begin{aligned}
i\mathcal{M}^{(l)} = &-g^W_{\sigma_1} \left(g^W_{\sigma_3} \right)^2 g_{ZWW}\, D^W(k_1 + k_2)\, D^W(p_1 - p_2) F_0 \left\langle p_2 \left| (\sigma_\mu)_{\sigma_1} \right| p_1 \right\rangle \\
&\times \left[\left\langle p_4,\, k_1 + k_2 \left| (\sigma^\mu)_{\sigma_3} \right| p_3 \right\rangle \delta_{q_2,d} + \left\langle p_4 \left| (\sigma^\mu)_{\sigma_3} \right| k_1 + k_2,\, p_3 \right\rangle \delta_{q_2,u} \right] \qquad \text{(A20)}
\end{aligned}
$$

The complete matrix element, given by the sum of $\mathcal{M}^{(a)} ... \mathcal{M}^{(\ell)}$, must be antisymmetrized in (p_1, σ_1) (p_3, σ_3) or (p_2, σ_2) (p_4, σ_4), when identical flavors occur on the two incoming or outgoing fermion lines.

To include the subsequent decays $W^+ \to \ell^+ \nu$, and $Z \to \ell^+ \ell^-$, we replace

$$
\epsilon^\mu(k_1) \to \frac{g}{\sqrt{2}} \sqrt{4 \bar{\ell^+}^0 \bar{\nu}^0}\, D^W(\ell^+ + \nu) \delta_{\sigma_\nu \sigma_{\ell^+}} \left\langle \nu \left| (\sigma^\mu)_{\sigma_\nu} \right| \ell^+ \right\rangle \ , \qquad \text{(A21)}
$$

$$
\epsilon^\mu(k_2) \to g^Z_{\sigma_\ell}(\ell) \sqrt{4 \bar{\ell^+}^0 \bar{\ell^-}^0}\, D^Z(\ell^+ + \ell^-) \delta_{\sigma_{\ell^+} \sigma_{\ell^-}} \left\langle \ell^- \left| (\sigma^\mu)_{\sigma_\ell} \right| \ell^+ \right\rangle \qquad \text{(A22)}
$$

in the above expressions, and we must use the narrow-width approximation for the final state W and Z propagators otherwise we have to include additional Feynman graphs to preserve gauge invariance.

APPENDIX B

In this Appendix we present the invariant amplitudes for the processes

$$gg \to Zt\bar{t}g \,, \tag{B1a}$$

$$q\bar{q} \to Zt\bar{t}g \,, \tag{B1b}$$

$$gq(\bar{q}) \to Zt\bar{t}q(\bar{q}) \,. \tag{B1c}$$

The amplitudes in this Appendix are calculated using the spinor methods described in Ref. [28]. In this method, the invariant amplitude is calculated by performing 4×4 matrix multiplications over the propagators, polarization vectors and u and v spinors. This method is a simple and efficient technique for calculating squared amplitudes when massive fermions are present.

We define the fermion propagator as

$$D_f(p) = \left[\not{p} - m_f + i\Theta(p^2)\Gamma_f m_f\right]^{-1} \,, \tag{B2}$$

where Γ_f is the decay width of fermion f. The Z polarization vector is

$$\epsilon_Z^{f\mu} = \epsilon^\mu(Z)(g_V^f + g_A^f\gamma_5) \,, \tag{B3}$$

and the gluon polarization vectors are $\epsilon_i^\mu = \epsilon^\mu(q_i)$. The Z coupling strengths g_V^f and g_A^f are defined as

$$g_V^f = (g_+^Z(f) + g_-^Z(f))/2 \qquad g_A^f = (g_+^Z(f) - g_-^Z(f))/2 \tag{B4}$$

using the $g_\pm^Z(f)$ of Eq. (A6).

We first consider the process $gg \to Zt\bar{t}g$. The Feynman diagrams for this process are shown in Fig. 7. We take the Z boson and top-quark momenta to be outgoing, and the gluon momenta to be incoming. The amplitudes corresponding to the Feynman diagrams in Fig. 7, up to an overall coupling of $-g_s^3$, are

$$\mathcal{M}_a = \bar{u}(t)\not{\ell}_Z^t D_t(q_a+q_b+q_c-\bar{t})\not{\ell}_a D_t(q_b+q_c-\bar{t})\not{\ell}_b D_t(q_c-\bar{t})\not{\ell}_c v(\bar{t})(T^aT^bT^c)_{ij}$$

$$+\text{permutations of } (a,b,c) \tag{B5a}$$

$$\mathcal{M}_b = \bar{u}(t)\not{\ell}_a D_t(t-q_a)\not{\ell}_Z^t D_t(q_b+q_c-\bar{t})\not{\ell}_b D_t(q_c-\bar{t})\not{\ell}_c v(\bar{t})(T^aT^bT^c)_{ij}$$

$$+\text{permutations of } (a,b,c) \tag{B5b}$$

$$\mathcal{M}_c = \bar{u}(t)\not{\ell}_a D_t(t-q_a)\not{\ell}_b D_t(t-q_a-q_b)\not{\ell}_Z^t D_t(q_c-\bar{t})\not{\ell}_c v(\bar{t})(T^aT^bT^c)_{ij}$$

$$+\text{permutations of } (a,b,c) \tag{B5c}$$

$$\mathcal{M}_d = \bar{u}(t)\not{\ell}_a D_t(t-q_a)\not{\ell}_b D_t(t-q_a-q_b)\not{\ell}_c D_t(t-q_a-q_b-q_c)\not{\ell}_Z^t v(\bar{t})(T^aT^bT^c)_{ij}$$

$$+\text{permutations of } (a,b,c) \tag{B5d}$$

$$\mathcal{M}_e = \bar{u}(t)\not{\ell}_Z^t D_t(q_a+q_b+q_c-\bar{t})\not{\ell}_a D_t(q_b+q_c-\bar{t})\not{V}(b,c)v(\bar{t})(T^a[T^b,T^c])_{ij}$$

$$+\text{cyclic permutations of } (a,b,c) \tag{B5e}$$

$$\mathcal{M}_f = \bar{u}(t)\not{\ell}_Z^t D_t(q_a+q_b+q_c-\bar{t})\not{V}(b,c)D_t(q_a-\bar{t})\not{\ell}_a v(\bar{t})([T^b,T^c]T^a)_{ij}$$

$$+\text{cyclic permutations of } (a,b,c) \tag{B5f}$$

$$\mathcal{M}_g = \bar{u}(t)\not{\ell}_a D_t(t-q_a)\not{\ell}_Z^t D_t(q_b+q_c-\bar{t})\not{V}(b,c)v(\bar{t})(T^a[T^b,T^c])_{ij}$$

$$+\text{cyclic permutations of } (a,b,c) \tag{B5g}$$

$$\mathcal{M}_h = \bar{u}(t)\not{V}(b,c)D_t(t-q_b-q_c)\not{\ell}_Z^t D_t(q_a-\bar{t})\not{\ell}_a v(\bar{t})([T^b,T^c]T^a)_{ij}$$

$$+\text{cyclic permutations of } (a,b,c) \tag{B5h}$$

$$\mathcal{M}_i = \bar{u}(t)\not{\ell}_a D_t(t-q_a)\not{V}(b,c)D_t(t-q_a-q_b-q_c)\not{\ell}_Z^t v(\bar{t})(T^a[T^b,T^c])_{ij}$$

$$+\text{cyclic permutations of } (a,b,c) \tag{B5i}$$

$$\mathcal{M}_j = \bar{u}(t)\not{V}(b,c)D_t(t-q_b-q_c)\not{\ell}_a D_t(t-q_a-q_b-q_c)\not{\ell}_Z^t v(\bar{t})([T^b,T^c]T^a)_{ij}$$

$$+\text{cyclic permutations of } (a,b,c) \tag{B5j}$$

$$\mathcal{M}_k = \bar{u}(t)\not{\ell}_Z^t D_t(q_a+q_b+q_c-\bar{t})\not{T}(a,b,c)v(\bar{t})[T^a,[T^b,T^c]]_{ij}$$

$$+\text{cyclic permutations of } (a,b,c) \tag{B5k}$$

$$\mathcal{M}_\ell = \bar{u}(t)\not{T}(a,b,c)D_t(t-q_a-q_b-q_c)\not{\ell}_Z^t v(\bar{t})[T^a,[T^b,T^c]]_{ij}$$

$$+\text{cyclic permutations of } (a,b,c) \tag{B5l}$$

$$\mathcal{M}_m = \bar{u}(t)\not{\epsilon}_Z^t D_t(q_a+q_b+q_c-\bar{t})\not{V}(a,b,c)v(\bar{t}) \tag{B5m}$$

$$\mathcal{M}_n = \bar{u}(t)\not{V}(a,b,c)D_t(t-q_a-q_b-q_c)\not{\epsilon}_Z^t v(\bar{t}) \tag{B5n}$$

where

$$\Gamma^\mu(a,b) = \left[-(2q_a+q_b)\cdot\epsilon_b\epsilon_a^\mu + (2q_b+q_a)\cdot\epsilon_a\epsilon_b^\mu + (q_a-q_b)^\mu\epsilon_a\cdot\epsilon_b\right]\Big/(q_a+q_b)^2 \tag{B6a}$$

$$\begin{aligned} T^\mu(a,b,c) = \Big[&-2q_a\cdot\Gamma(b,c)\epsilon_a^\mu + 2(q_b+q_c)\cdot\epsilon_a\Gamma^\mu(b,c) \\ &+ (q_a-q_b-q_c)^\mu\epsilon_a\cdot\Gamma(b,c)\Big]\Big/(q_a+q_b+q_c)^2 \end{aligned} \tag{B6b}$$

and

$$\begin{aligned} V^\mu(a,b,c) = \Big[&[[T^c,T^b],T^a]_{ij}(\epsilon_a\cdot\epsilon_c\epsilon_b^\mu - \epsilon_a\cdot\epsilon_b\epsilon_c^\mu) + [T^b,[T^a,T^c]]_{ij}(\epsilon_a\cdot\epsilon_b\epsilon_c^\mu - \epsilon_a^\mu\epsilon_b\cdot\epsilon_c) \\ &+ [T^c,[T^a,T^b]]_{ij}(\epsilon_a^\mu\epsilon_b\cdot\epsilon_c - \epsilon_a\cdot\epsilon_c\epsilon_b^\mu)\Big]\Big/(q_a+q_b+q_c)^2\,. \end{aligned} \tag{B6c}$$

The color sum, which involves the T_{ij}^a type terms, was performed using the method of Ref [29]. Analytic expressions for the color sum are given in Ref. [19].

There are 24 contributing Feynman diagrams to the process $q\bar{q} \to Zt\bar{t}g$ shown in Fig. 8. To present the invariant amplitudes we define

$$u_{1V} = \frac{(\not{p}_1 - \not{p}_V)}{(p_1-p_V)^2}\not{\epsilon}_V u(p_1) \tag{B7a}$$

$$\bar{v}_{2V} = \bar{v}(p_2)\not{\epsilon}_V\frac{(\not{p}_V - \not{p}_2)}{(p_V-p_2)^2} \tag{B7b}$$

$$\bar{u}_{3V} = \bar{u}(p_3)\not{\epsilon}_V\frac{(\not{p}_3 + \not{p}_V + m_t)}{(p_3+p_V)^2 - m_t^2 + i\Gamma_t m_t} \tag{B7c}$$

$$v_{4V} = \frac{(-\not{p}_4 - \not{p}_V + m_t)}{(p_4+p_V)^2 - m_t^2 + i\Gamma_t m_t}\not{\epsilon}_V v(p_4) \tag{B7d}$$

$$\text{where } p_V = \begin{cases} p_5\,, & V = g \\ p_6\,, & V = Z \end{cases} \tag{B8}$$

$$\text{and where } \epsilon_V = \begin{cases} \epsilon(p_5)\,, & V = g \\ \epsilon_Z^f\,, & V = Z \end{cases} \tag{B9}$$

with $\epsilon_Z^f = \epsilon(p_6)(g_V^f + g_A^f\gamma_5)$, with f being the appropriate quark flavor. We define the quark currents

$$J_{21}^\mu = \bar{v}(p_2)\gamma^\mu u(p_1)/(p_1+p_2)^2\,, \qquad J_{34}^\mu = \bar{u}(p_3)\gamma^\mu v(p_4)/(p_3+p_4)^2 \tag{B10}$$

and the three gluon coupling as

$$\Gamma^\mu(\epsilon_1,q_1,\epsilon_2,q_2) = [-(2q_1+q_2)\cdot\epsilon_2\epsilon_1^\mu + (2q_2+q_1)\cdot\epsilon_1\epsilon_2^\mu + (q_1-q_2)^\mu\epsilon_1\cdot\epsilon_2]\Big/(q_1+q_2)^2\,. \tag{B11}$$

Using these definitions, the invariant amplitudes corresponding to the diagrams in Figure 8 are, up to an overall coupling factor g_s^3 and the color factors,

$$\mathcal{M}_a = \bar{u}_{3Z}\gamma^\mu v(p_4)\bar{v}_{2g}\gamma_\mu u(p_1)(p_3+p_4+p_6)^{-2} \tag{B12a}$$

$$\mathcal{M}_b = \bar{u}(p_3)\gamma^\mu v_{4Z}\bar{v}_{2g}\gamma_\mu u(p_1)(p_3+p_4+p_6)^{-2} \tag{B12b}$$

$$\mathcal{M}_c = \bar{v}_{2g}\not{J}_{34}u_{1Z} \tag{B12c}$$

$$\mathcal{M}_d = \bar{v}_{2g}\not{\epsilon}_Z^q D_q(p_1-p_3-p_4)\not{J}_{34}u(p_1) \tag{B12d}$$

$$\mathcal{M}_e = \bar{v}_{2Z}\not{\epsilon}(p_5)D_q(p_1-p_3-p_4)\not{J}_{34}u(p_1) \tag{B12e}$$

$$\mathcal{M}_f = \bar{v}(p_2)\not{J}_{34}D_q(p_3+p_4-p_2)\not{\epsilon}(p_5)u_{1Z} \tag{B12f}$$

$$\mathcal{M}_g = \bar{v}(p_2)\not{J}_{34}D_q(p_3+p_4-p_2)\not{\epsilon}_Z^q u_{1g} \tag{B12g}$$

$$\mathcal{M}_h = \bar{v}(p_2)\gamma_\mu u_{1g}\bar{u}_{3Z}\gamma^\mu v(p_4)(p_3+p_4+p_6)^{-2} \tag{B12h}$$

$$\mathcal{M}_i = \bar{v}(p_2)\gamma_\mu u_{1g}\bar{u}(p_3)\gamma^\mu v_{4Z}(p_3+p_4+p_6)^{-2} \tag{B12i}$$

$$\mathcal{M}_j = \bar{v}_{2Z}\not{J}_{34}u_{1g} \tag{B12j}$$

$$\mathcal{M}_k = \bar{v}(p_2)\not{V}(\bar{u}_{3Z}\gamma^\mu v(p_4),(p_3+p_4+p_6),\epsilon(p_5),p_5)u(p_1) \tag{B12k}$$

$$\mathcal{M}_l = \bar{v}(p_2)\not{V}(\bar{u}(p_3)\gamma^\mu v_{4Z},(p_3+p_4+p_6),\epsilon(p_5),p_5)u(p_1) \tag{B12l}$$

$$\mathcal{M}_m = \bar{v}(p_2)\not{V}(\bar{u}(p_3)\gamma^\mu v(p_4),(p_3+p_4),\epsilon(p_5),p_5)D_q(p_1-p_6)\not{\ell}^q_Z u(p_1) \tag{B12m}$$

$$\mathcal{M}_n = \bar{v}(p_2)\not{\ell}^q_Z D_q(p_6-p_2)\not{V}(\bar{u}(p_3)\gamma^\mu v(p_4),(p_3+p_4),\epsilon(p_5),p_5)u(p_1) \tag{B12n}$$

$$\mathcal{M}_o = \bar{u}_{3Z}\not{\epsilon}(p_5)D_t(p_3+p_5+p_6)\not{J}_{21}v(p_4) \tag{B12o}$$

$$\mathcal{M}_p = \bar{u}_{3g}\not{\ell}^t_Z D_t(p_3+p_5+p_6)\not{J}_{21}v(p_4) \tag{B12p}$$

$$\mathcal{M}_q = \bar{u}_{3g}\not{J}_{21}v_{4Z} \tag{B12q}$$

$$\mathcal{M}_r = \bar{v}(p_2)\gamma^\mu u_{1Z}\bar{u}_{3g}\gamma_\mu v(p_4)(p_3+p_4+p_5)^{-2} \tag{B12r}$$

$$\mathcal{M}_s = \bar{v}_{2Z}\gamma^\mu u(p_1)\bar{u}_{3g}\gamma_\mu v(p_4)(p_3+p_4+p_5)^{-2} \tag{B12s}$$

$$\mathcal{M}_t = \bar{u}_{3Z}\not{J}_{21}v_{4g} \tag{B12t}$$

$$\mathcal{M}_u = \bar{u}(p_3)\not{J}_{21}D_t(-p_4-p_5-p_6)\not{\ell}^t_Z v_{4g} \tag{B12u}$$

$$\mathcal{M}_v = \bar{u}(p_3)\not{J}_{21}D_t(-p_4-p_5-p_6)\not{\epsilon}(p_5)v_{4Z} \tag{B12v}$$

$$\mathcal{M}_w = \bar{v}(p_2)\gamma^\mu u_{1Z}\bar{u}(p_3)\gamma_\mu v_{4g}(p_3+p_4+p_5)^{-2} \tag{B12w}$$

$$\mathcal{M}_x = \bar{v}_{2Z}\gamma^\mu u(p_1)\bar{u}(p_3)\gamma_\mu v_{4g}(p_3+p_4+p_5)^{-2}\ . \tag{B12x}$$

The amplitude squared, summed over color, is

$$|\mathcal{M}|^2 = |\mathcal{M}_1+\mathcal{M}_2-\mathcal{M}_4-\mathcal{M}_5|^2/6+|\mathcal{M}_1+\mathcal{M}_2+\mathcal{M}_4+\mathcal{M}_5|^2+3|\mathcal{M}_1-\mathcal{M}_2+2\mathcal{M}_3-\mathcal{M}_4+\mathcal{M}_5|^2/2 \tag{B13}$$

where

$$\mathcal{M}_1 = \mathcal{M}_a+\ldots+\mathcal{M}_e \tag{B14a}$$

$$\mathcal{M}_2 = \mathcal{M}_f+\ldots+\mathcal{M}_j \tag{B14b}$$

$$\mathcal{M}_3 = \mathcal{M}_k+\ldots+\mathcal{M}_n \tag{B14c}$$

$$\mathcal{M}_4 = \mathcal{M}_o+\ldots+\mathcal{M}_s \tag{B14d}$$

$$\mathcal{M}_5 = \mathcal{M}_t+\ldots+\mathcal{M}_x \tag{B14e}$$

The amplitude squared for the the process $gq(\bar{q}) \to Zt\bar{t}q(\bar{q})$ is straightforwardly obtained

from Eq. (B13) by crossing the final gluon with either the initial quark or antiquark in the amplitudes $\mathcal{M}_a$ through $\mathcal{M}_x$.

In the above invariant amplitudes, the Z-boson is decayed into fermions by the substitution

$$\epsilon^\mu(Z) \to -\frac{\bar{u}(f)\gamma^\mu(g_V^f + g_A^f\gamma_5)v(\bar{f})}{Z^2 - M_Z^2 + iM_Z\Gamma_Z} \tag{B15}$$

where f and $\bar{f}$ denote fermion momenta and Γ_Z is the decay width of the Z boson. Similarly, the top and anti-top quarks are decayed by the substitution

$$\bar{u}(t) \to \frac{g}{\sqrt{2}}\bar{u}(b)\not{\epsilon}(W)P_- \frac{(\not{t} + m_t)}{t^2 - m_t^2 + im_t\Gamma_t} \tag{B16}$$

for the decay $t \to W^+b$, with $P_- = \frac{1}{2}(1 - \gamma_5)$, and

$$\bar{u}(t) = \frac{-g^2}{2}\bar{u}(b)\gamma_\mu P_- \frac{(\not{t} + m_t)}{t^2 - m_t^2 + im_t\Gamma_t} \frac{\bar{u}(\nu)\gamma^\mu P_- v(e^+)}{W^2 - M_W^2 + iM_W\Gamma_W} \tag{B17}$$

for the decay $t \to \nu e^+ b$. For anti-top quark decay we substitute

$$v(\bar{t}) = \frac{g}{\sqrt{2}} \frac{(-\not{\bar{t}} + m_t)}{\bar{t}^2 - m_t^2 + im_t\Gamma_t}\not{\epsilon}(W)P_- v(\bar{b}) \tag{B18}$$

and

$$v(\bar{t}) = \frac{-g^2}{2} \frac{(-\not{\bar{t}} + m_t)}{\bar{t}^2 - m_t^2 + im_t\Gamma_t}\gamma_\mu P_- v(\bar{b}) \frac{\bar{u}(e^-)\gamma^\mu P_- v(\nu)}{W^2 - M_W^2 + iM_W\Gamma_W} \tag{B19}$$

for $\bar{t} \to W^-\bar{b}$ and $\bar{t} \to e^-\bar{\nu}\bar{b}$, respectively. Gauge dependent terms in the W-boson propagator are removed by the Dirac equation for the massless neutrino and electron.

The numerical program based on the formulas in this Appendix was tested extensively. In the limit $m_t \to 0$ it agrees with the results of Refs. [19, 30]. In addition, the gauge invariance of the amplitudes and the Lorentz invariance of the resulting cross sections were verified numerically.

REFERENCES

[1] D. Zeppenfeld and S. Willenbrock, Phys. Rev. **D37**, 1775 (1988); G. Martinelli *et al.*, in *Proceedings of the LH Workshop*, Vol II, p. 91, Aachen, Germany (1990), edited by G. Jarlskog and D. Rein.

[2] B. W. Lee, C. Quigg, and H. B. Thacker, Phys. Rev. **D16**, 1519 (1977); M. S. Chanowitz and M. K. Gaillard, Nucl. Phys. **B261**, 375 (1985); M. S. Chanowitz, Ann. Rev. Nucl. Part. Sci. **38**, 323 (1985).

[3] R. N. Cahn and S. Dawson, Phys. Lett. **136B**, 196 (1984); J. F. Gunion, Z. Kunszt, and M. Soldate, Phys. Lett. **163B**, 389 (1985); **168B**, 427(E) (1986); J. F. Gunion and M. Soldate, Phys. Rev. **D34**, 826 (1986); J. F. Gunion *et al.*, R. N. Cahn *et al.*, Phys. Rev. **D35**, 1626 (1987); V. Barger, T. Han, and R. J. N. Phillips, Phys. Rev. **D37** 2005 (1988); R. N. Cahn *et al.*, in *Proceedings of Workshop on Experiments, Detectors, and Experimental Areas for the SSC*, Berkeley, CA, Jul. 7, 1987; R. Kleiss and W. J. Stirling, Phys. Lett. **200B**, 193 (1988); V. Barger, T. Han, and R. J. N. Phillips, Phys. Lett. **200B**, 193 (1988); G. Kane and C. P. Yuan, Phys. Rev. **D40**, 2231 (1989); J. F. Gunion, G. L. Kane, H. E. Haber, and S. Dawson, *The Higgs Hunter's Guide*, Addison Wesley (1989). UC-Davis report UCD-91-0010 (1990), in *Research Directions for the Decade*, Proceedings of the Workshop, Snowmass, Colorado (1990), (Editions Frontières, Gif-sur-Yvette, France, in press); V. Barger, in *Proceedings of the International Conference on High Energy Physics, Beyond the Standard Model II*, Norman, Oklahoma (1990), edited by K. Milton, R. Kantowski, and M. Samuel; D. Froidevaux, in *Proceedings of the LHC Workshop*, Vol. II, p. 444, Aachen, Germany (1990), edited by G. Jarlskog and D. Rein.

[4] U. Baur and E. W. N. Glover, Nucl. Phys. **B347**, 12 (1990).

[5] V. Barger, K. Cheung, T. Han, J. Ohnemus, and D. Zeppenfeld, Phys. Rev. **D44**, 1426 (1991).

[6] V. Barger, K. Cheung, T. Han, and D. Zeppenfeld, Phys. Rev. **D44**, 2701 (1991).

[7] M. S. Chanowitz and M. Golden, Phys. Rev. Lett. **61**, 1053 (1988); **63**, 466(E) (1989).

[8] V. Barger, K. Cheung, T. Han, and R. J. N. Phillips, Phys. Rev. **D42**, 3052 (1990).

[9] D. Dicus, J. F. Gunion, R. Vega, Phys. Lett. **B258**, 475 (1991); D. Dicus, J. F. Gunion, L. H. Orr, and R. Vega, UC-Davis preprint, UCD-91-10, (1991).

[10] M. S. Chanowitz and M. S. Berger, Phys. Lett. **B263**, 509 (1991); M. S. Berger and M. S. Chanowitz, LBL-30476 (1991).

[11] D. Dicus and R. Vega, Phys. Lett. **217**, 194 (1989).

[12] See, for example E. Farhi and L. Susskind, Phys. Rept. **74**, 277 (1981); T. Appelquist, in *Proceedings of Grand Unification*, p. 123, Chapel Hill, (1989).

[13] A. Dobado, M. J. Herrero, and T. N. Truong, Phys. Lett. **235**, 129 (1990); A. Dobado, M. J. Herrero, and T. N. Truong, Z. Phys. **C50**, 465 (1991).

[14] J. Bagger, T. Han, and R. Rosenfeld, Fermilab preprint FERMILAB-CONF-90/253-T, to appear in *Proceedings of the 1990 DPF Summer Study on High Energy Physics: Research Directions for the Decade*, Snowmass, CO, 1990.

[15] R. Casalbuoni *et al.*, Phys. Lett. **B249**, 130 (1990); R. Casalbuoni *et al., ibid*, **253**, 275 (1991).

[16] R. W. Brown, D. Sahdev, and K. O. Mikaelian, Phys. Rev. **D20**, 1164 (1979); E. Eichten *et al.*, Rev. Mod. Phys. **56**, 579 (1984), erratum, **58**, 1065 (1986).

[17] J. Ohnemus, Fermilab preprint, FERMILAB-PUB-91/163-T, to appear in Phys. Rev. **D**.

[18] K. Hagiwara and D. Zeppenfeld, Nucl. Phys. **B274**, 1 (1986).

[19] K. Hagiwara and D. Zeppenfeld, Nucl. Phys. **B313**, 560 (1989).

[20] A. Bodek *et al.*, Phys. Rev. **D20**, 1471 (1979); S. Stein *et al.*, Phys. Rev. **D12**, 1884 (1975).

[21] U. Baur, J. Vermaseren, and D. Zeppenfeld, UW-Madison preprint, MAD/PH/675 (1991).

[22] P. N. Harriman, A. D. Martin, R. G. Roberts, and W. J. Stirling, Phys. Rev. **D42**, 798 (1990).

[23] U. Baur, E. W. N. Glover, and J. J. van der Bij, Nucl. Phys. **B318**, 106 (1989).

[24] V. Barger, T. Han, J. Ohnemus, and D. Zeppenfeld, Phys. Rev. **D41**, 2782 (1990).

[25] V. Barger, A. Stange, and R. J. N. Phillips, UW-Madison preprint, MAD/PH/644 (1991).

[26] V. Barger and R. J. N. Phillips, Phys. Rev. Lett. **55**, 2752 (1985); H. Baer, V. Barger, H. Goldberg, and R. J. N. Phillips, Phys. Rev. **D37**, 3152 (1988).

[27] V. Barger, A. D. Martin, and R. J. N. Phillips, Phys. Lett. **B125**, 339 (1983); V. Barger, T. Han, and J. Ohnemus, Phys. Rev. **D37**, 1174 (1988).

[28] V. Barger, R. J. N. Phillips and A. L. Stange, Phys. Rev. **D44**, 1987 (1991).

[29] V. Barger, R. J. N. Phillips and A. L. Stange, UW–Madison preprint, MAD/PH/621 (1991).

[30] V. Barger, T. Han, J. Ohnemus and D. Zeppenfeld, Phys. Rev. **D40**, 2888 (1989).

TABLES

TABLE I. Cross sections in fb for the EW signal and backgrounds (with $m_t = 140$ GeV), after requiring a jet in the forward region with $p_{Tj}(\text{tag}) > 40$ GeV, and $3 < |\eta_j(\text{tag})| < 5$. Leptonic acceptance cuts are $p_T(\ell) > 25$ GeV and $|y_\ell| < 2$. The four leptonic channels ($\bar{\ell}_1\ell_2\ell_3\nu$, where $\ell_i = e, \mu$) are summed.

	EW	$Zt\bar{t}g$'	QCD
(1) $E_j(\text{tag}) > 0.4$ TeV	6.8	9.3	7.1
(2) $E_j(\text{tag}) > 2$ TeV	4.8	3.7	2.1
(3) $n_j(\text{central}) \leq 1$ $E_j(\text{tag}) > 0.4$ TeV	6.8	2.6	7.1
(4) $n_j(\text{central}) \leq 1$ $E_j(\text{tag}) > 2$ TeV	4.8	1.0	2.1
(5) same as (4) plus $M(\ell\ell\ell) > 300$ GeV	2.0	0.5	0.4

TABLE II. Cross sections in fb for the signal with $m_H = 0.1$ and 1 TeV, after tagging a forward jet ($E_j(\text{tag}) > 2$ TeV, $p_{Tj}(\text{tag}) > 40$ GeV, $3 < |\eta_j(\text{tag})| < 5$). Here $n_j(\text{central})$ denotes the allowed number of central jets after additional vetoing of jets with $p_T(j) > 40$ GeV and $|\eta_j| < 3$. The leptonic acceptance criteria are the same as in Table I.

	$m_H = 0.1$ TeV	$m_H = 1$ TeV
$n_j(\text{central}) \leq 1$	4.8	5.1
$n_j(\text{central}) = 0$	1.6	1.8

FIGURES

FIG. 1. Feynman graphs for the electroweak process $qq \to qqW^{\pm}Z$. Representative diagrams are shown for (a) vector boson fusion, (b) t-channel γ, Z and W exchange, and (c) s-channel electroweak boson exchange.

FIG. 2. Energy distribution of the forward tagged jet with $3 < |\eta_j(\text{tag})| < 5$ and $p_{Tj}(\text{tag}) > 40$ GeV. The EW signal assumes $m_H = 0.1$ TeV. The leptonic acceptance criteria are $p_T(\ell) > 25$ GeV and $|y_\ell| < 2$. Also shown are the backgrounds from $Zt\bar{t}$'g' (with $m_t = 140$ GeV) production and from the QCD correction to $q\bar{q} \to WZ$ annihilation: see Eq. (1).

FIG. 3. Energy distribution of the forward tagged jet with additional veto of events with more than one central jet with $|\eta_j| < 3$ and $p_{Tj} > 40$ GeV. Other requirements are as in Fig. 2.

FIG. 4. Cluster transverse mass distribution of $W^{\pm}Z$ events for the EW $qq \to qqWZ$ signal (with $m_H = 0.1$ TeV) and the $Zt\bar{t}$'g' and QCD backgrounds. Acceptance criteria are as in Fig. 3 except for an additional missing transverse momentum cut of $\not{p}_T > 75$ GeV and $E_j(\text{tag}) > 2$ TeV.

FIG. 5. Invariant mass distribution of the three charged leptons $M(\ell\ell\ell)$ for the $qq \to qqWZ$ signal (with $m_H = 0.1$ TeV) and the $Zt\bar{t}$'g' and QCD backgrounds. Acceptance criteria are the same as in Fig. 3, plus $E_j(\text{tag}) > 2$ TeV.

FIG. 6. Feynman graphs for the electroweak $qq \to qqW^+Z$ process at order α^4 in R_ξ gauge.

FIG. 7. Feynman graphs for the $gg \to Zt\bar{t}g$ subprocess.

FIG. 8. Feynman graphs for the $q\bar{q} \to Zt\bar{t}g$ subprocess.

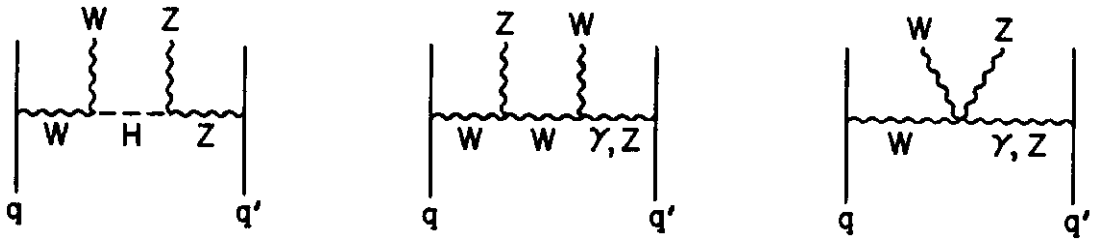

(a)

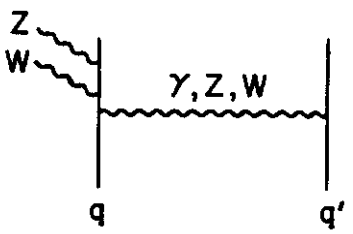

(b)

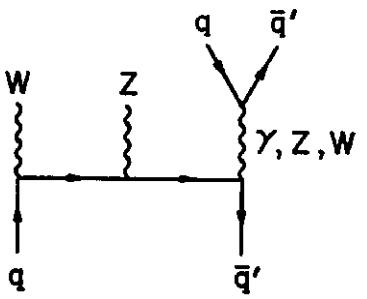

(c)

Fig. 1

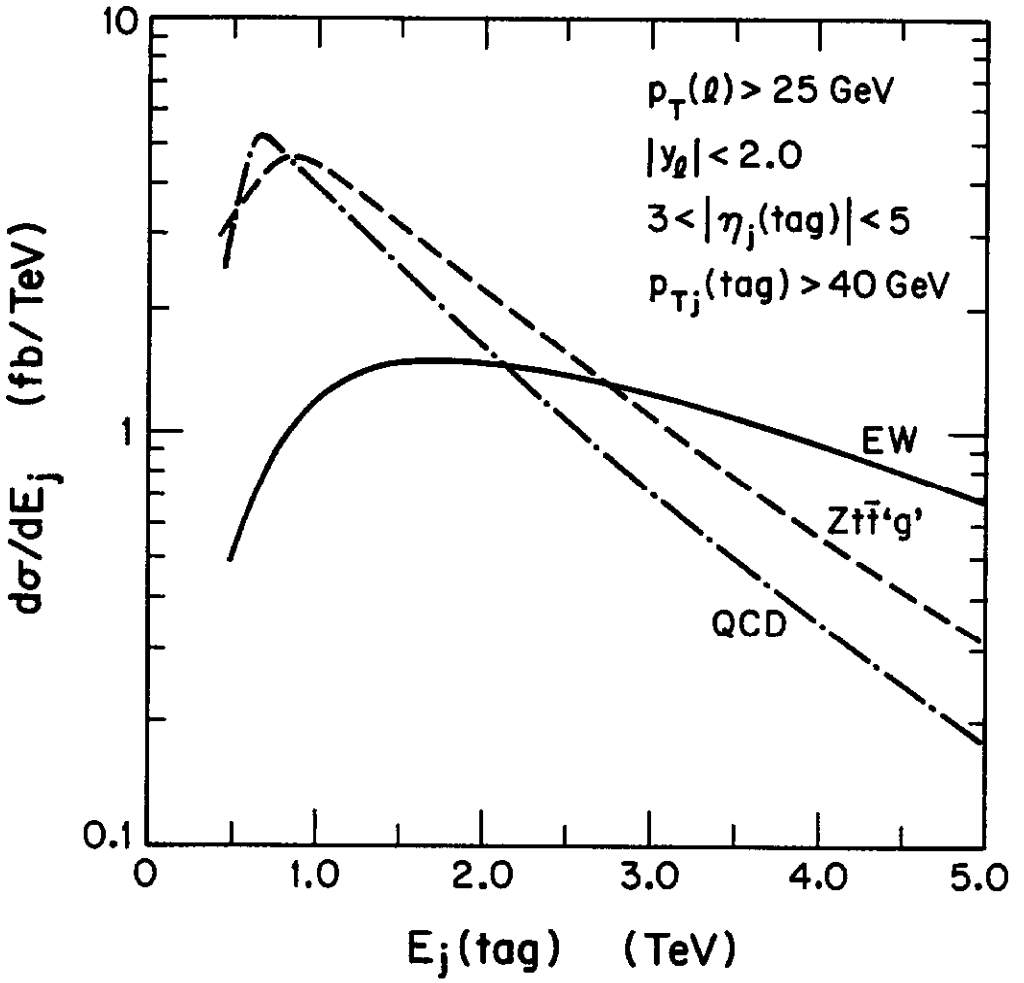
10
1
0.1
0
1.0
2.0
3.0
4.0
5.0
$d\sigma/dE_j$ (fb/TeV)
E_j(tag) (TeV)
$p_T(\ell) > 25$ GeV
$|y_\ell| < 2.0$
$3 < |\eta_j(\text{tag})| < 5$
$p_{Tj}(\text{tag}) > 40$ GeV
EW
$Zt\bar{t}g$
QCD

Fig. 2

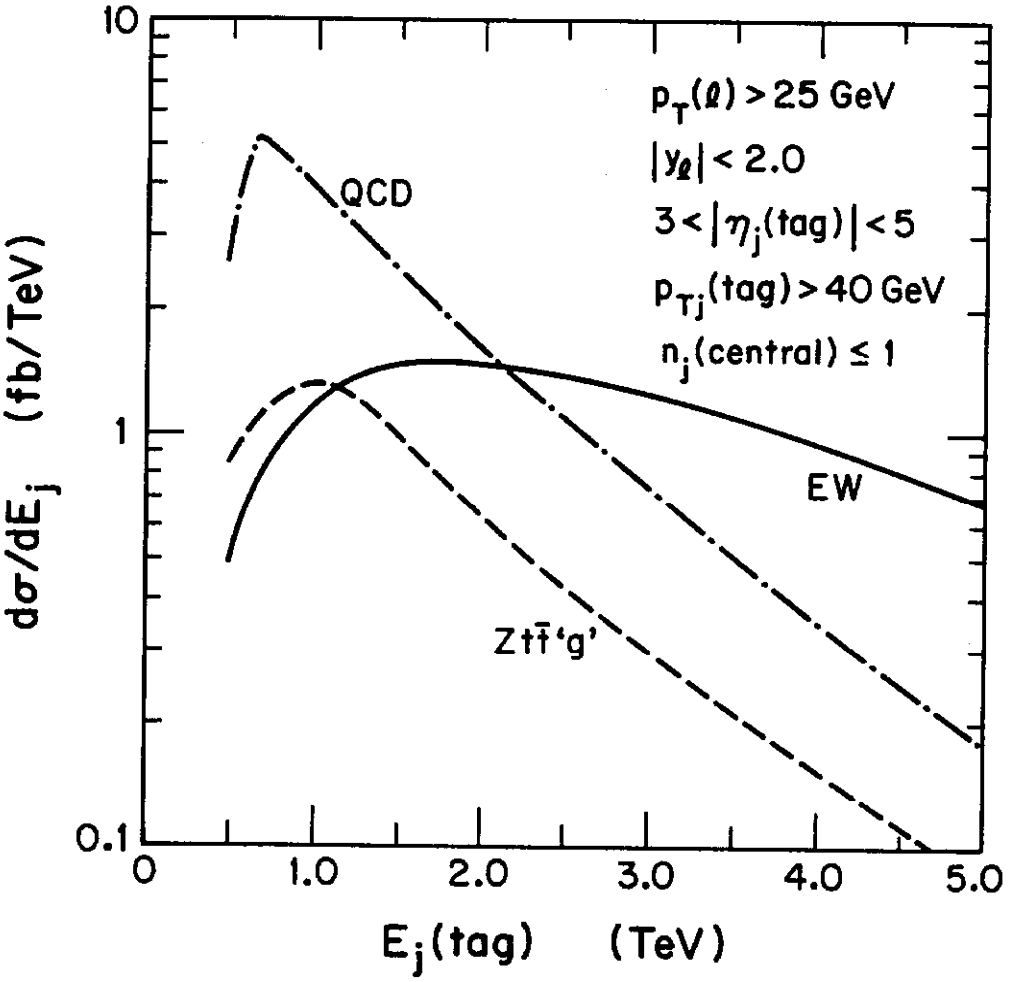
10
1
0.1
0
1.0
2.0
3.0
4.0
5.0
$d\sigma/dE_j$ (fb/TeV)
E_j(tag) (TeV)
$p_T(\ell) > 25$ GeV
$|y_\ell| < 2.0$
$3 < |\eta_j(\text{tag})| < 5$
$p_{Tj}(\text{tag}) > 40$ GeV
$n_j(\text{central}) \leq 1$
QCD
EW
$Zt\bar{t}$'g'

Fig. 3

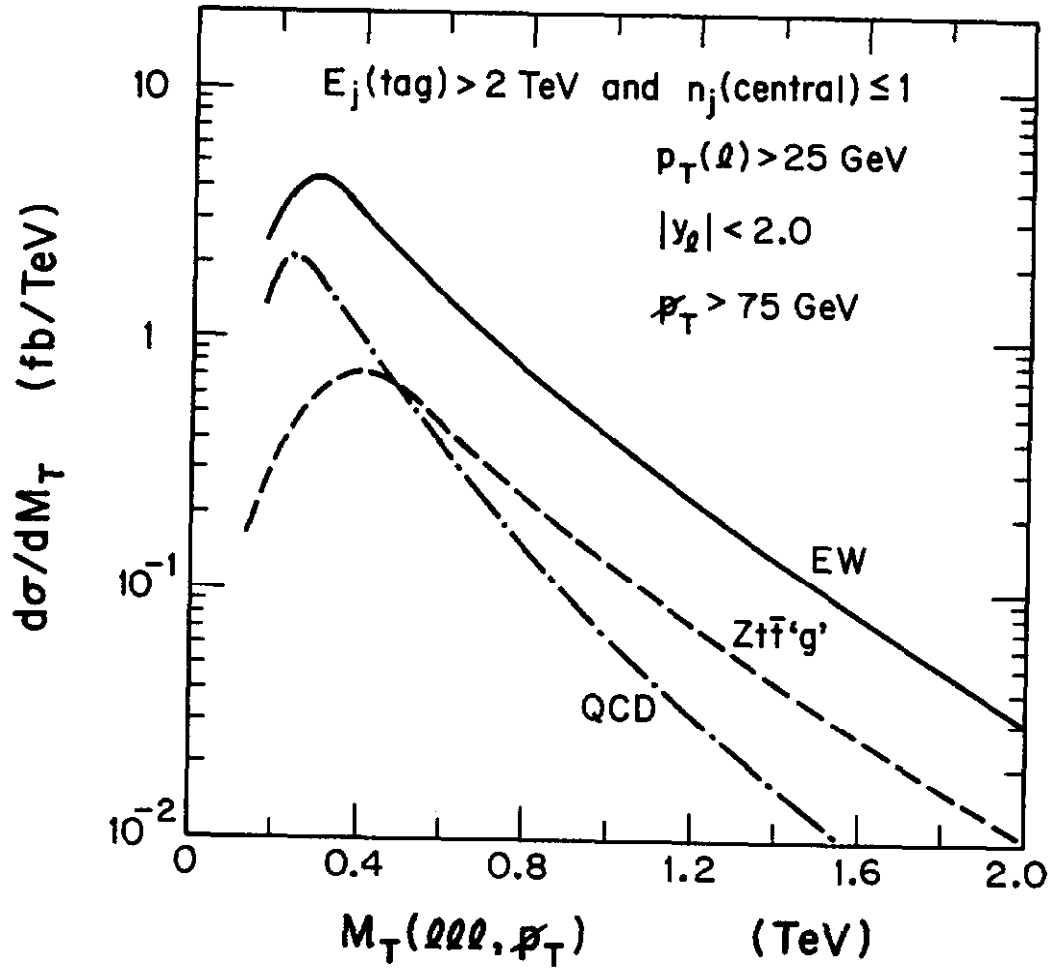
$E_j(tag) > 2$ TeV and $n_j(central) \leq 1$
$p_T(\ell) > 25$ GeV
$|y_\ell| < 2.0$
$\not{p}_T > 75$ GeV
EW
$Zt\bar{t}$'g'
QCD
$d\sigma/dM_T$ (fb/TeV)
$M_T(\ell\ell\ell, \not{p}_T)$ (TeV)
10
1
10^{-1}
10^{-2}
0
0.4
0.8
1.2
1.6
2.0

Fig. 4

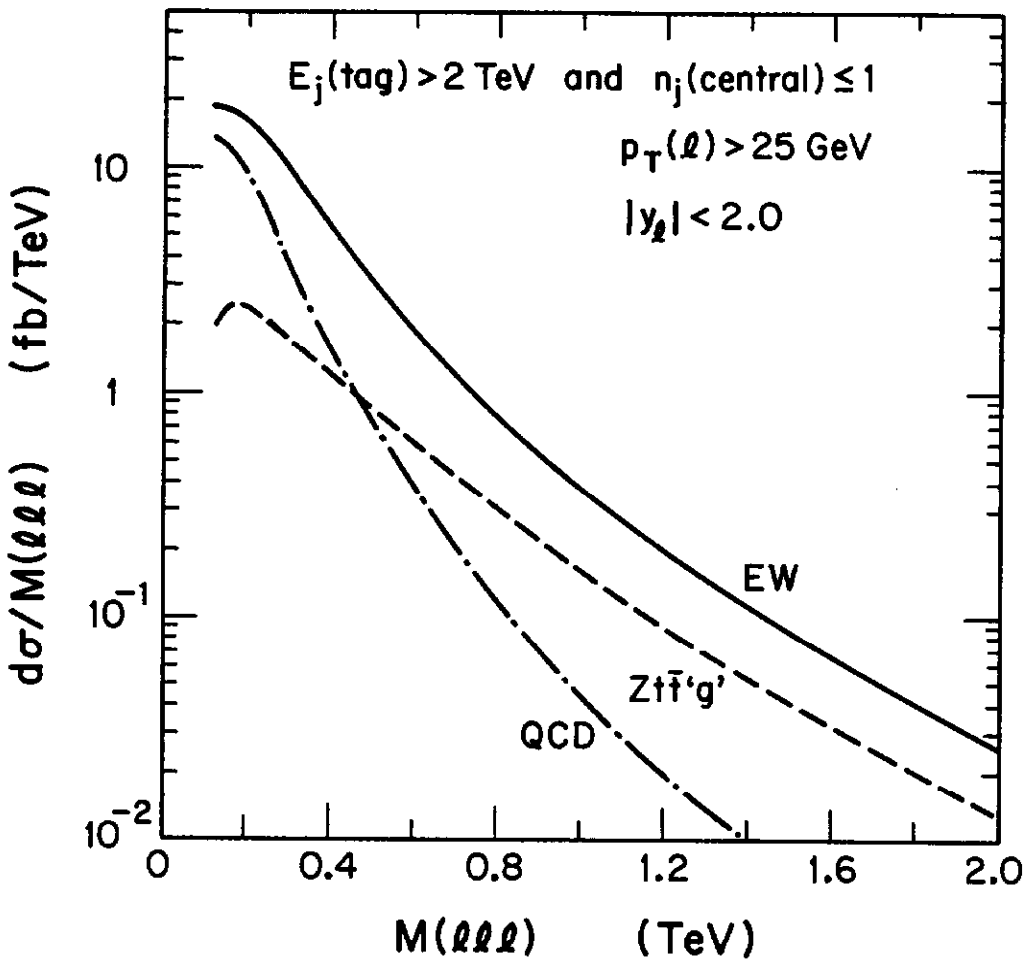
E_j(tag) > 2 TeV and n_j(central) ≤ 1
$p_T(\ell) > 25$ GeV
$|y_\ell| < 2.0$
EW
$Zt\bar{t}$'g'
QCD
$d\sigma/M(\ell\ell\ell)$ (fb/TeV)
$M(\ell\ell\ell)$ (TeV)
10
1
10^{-1}
10^{-2}
0
0.4
0.8
1.2
1.6
2.0

Fig. 5

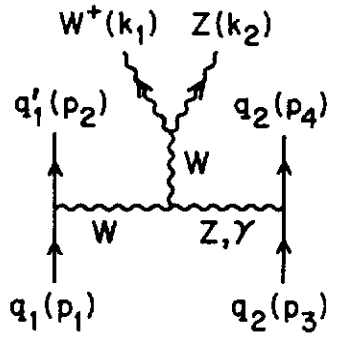

(a)

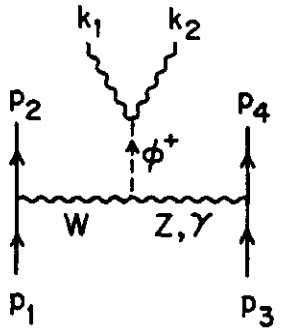

(b)

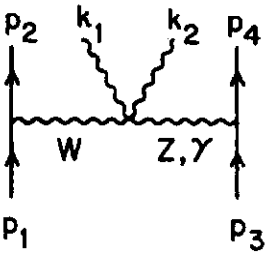

(c)

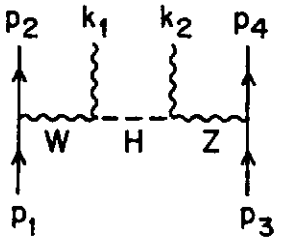

(d)

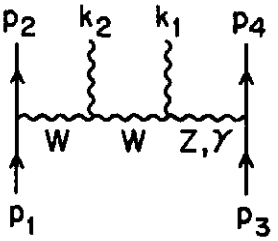

(e)

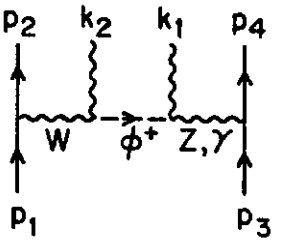

(f)

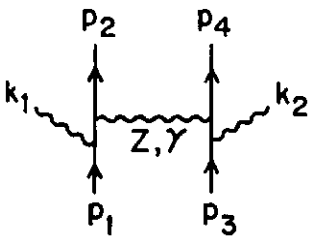

+ 9 permutations

(g)

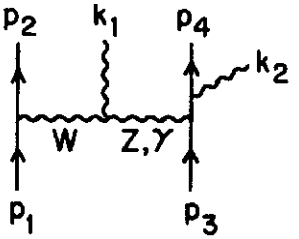

+ 3 permutations of k_2

(h)

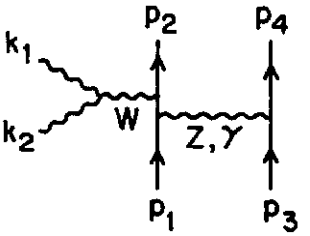

+ 1 permutation of W propagator

(i)

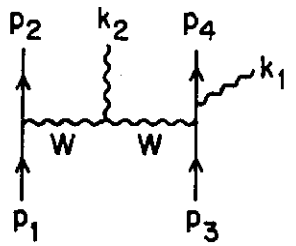

(j)

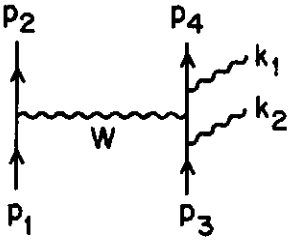

+ 4 permutations of k_2

(k)

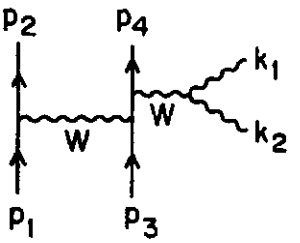

(l)

Fig. 6

Fig. 7

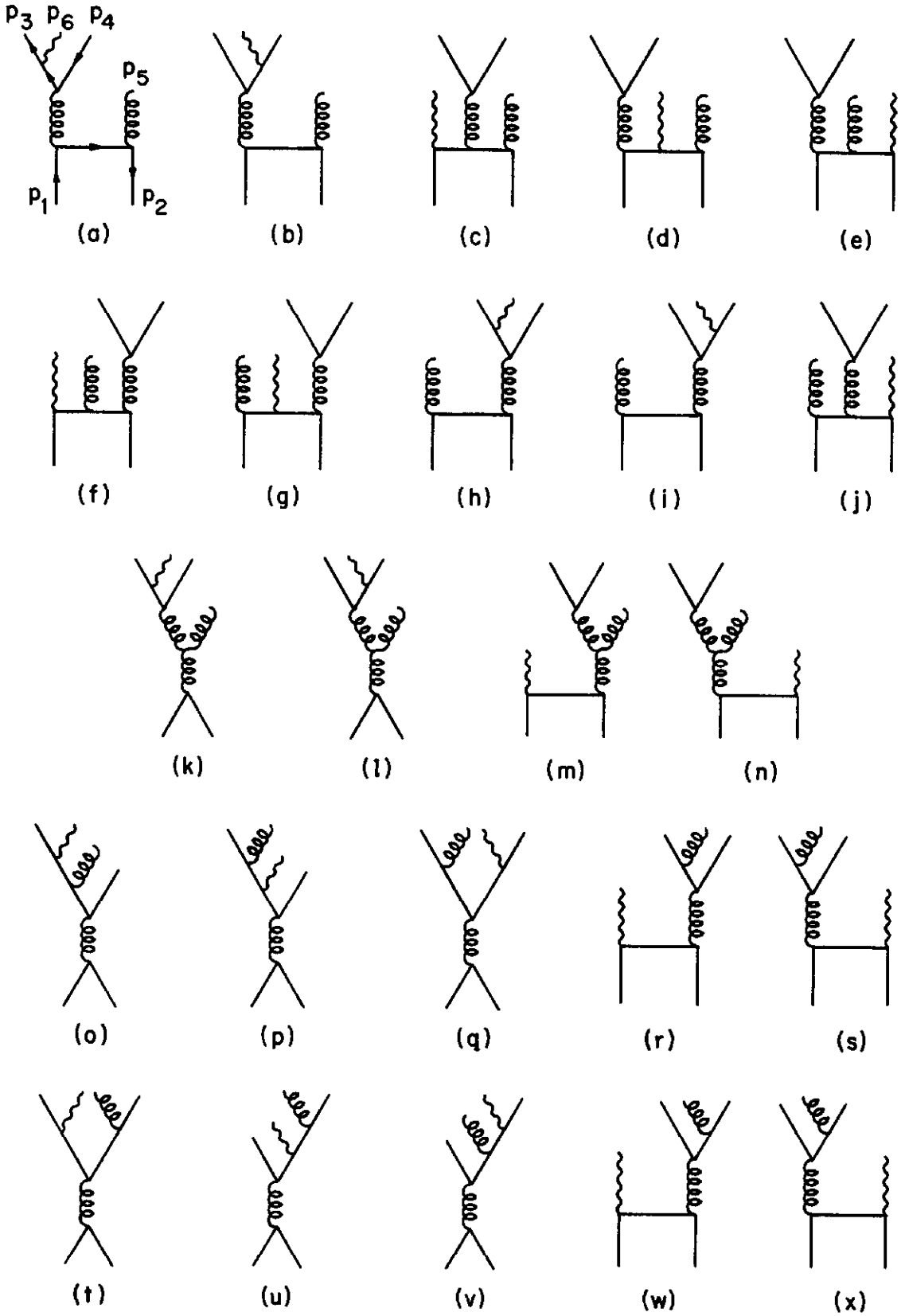

Fig. 8